Experimental and Analytical Investigation of Flow Through Rocket Pump Inducer[1]

B. LAKSHMINARAYANA

The Pennsylvania State University

A rocket pump inducer is usually an axial-flow pump runner having very high solidity and very low aspect ratio blades operating at very low coefficients. While this characteristic form is dictated by cavitation requirements, the flow is subjected to major effects of viscosity and turbulence in the flow field in the long and narrow passages between the vanes. The investigations reported in this paper are concerned with the effects of viscosity and not with the effects of cavitation.

The experimental investigations are carried out on a 3-foot-diameter model of a four-bladed inducer which is operated in air at a flow coefficient 0.065. The fluid properties are measured at the exit of the inducer using conventional and hot-wire probes. Important experimental results and the method of predicting the outlet tangential velocity and head rise are discussed in this paper.

One of the major requirements of a turbopump used in rocket application is that it should be capable of running at very high speeds, so as to minimize the size and weight of the unit and to facilitate matching with a drive turbine. The conventional pumps cavitate at suction specific speeds (SS) in excess of 8000, thus limiting the highest possible speed. The need to increase the speed led to the development of a cavitation resistance inducer which is essentially an axial-flow pump with high solidity blades used in front of the main pump. Long and narrow helical passages provide a space and time for the collapse of cavitation bubbles and for the gradual addition of energy to the fluid. Inducers are also used in water jet pumps of marine application (ref. 2). These are light and feature cavitation resistance in excess of commercial applications.

---

[1] The work reported here was done under contracts NSG537 and NGL 39–009–007 of the National Aeronautics and Space Administration, with technical management by W. R. Britsch of NASA Lewis Research Center.

The purpose of the inducer is to pressurize the flow sufficiently to enable the main pump to operate satisfactorily. The physical reasoning for the selection of such unconventional blade passages is explained by Acosta (ref. 1). These inducers have operated successfully at suction specific speeds in excess of 30 000; the test inducer described later is designed for SS = 50 000. The characteristic features of the inducers are:

(1) High solidity blading (few long-chord blades instead of many short-chord blades as in axial-flow pumps and compressors, exposing a much larger area to frictional effects)

(2) Very low flow coefficient and large stagger angles.

While the characteristic form of the inducer is dictated by cavitation requirements, the flow is subjected to major effects of viscosity and turbulence of the fluid in the long and narrow passages between the inducer vanes. The investigations reported here are concerned with the effects of viscosity and not with the effects of cavitation.

In axial-flow compressors or pumps, the secondary motions or the departure of the flow from design values are confined to fairly thin regions around the blades and near the end walls. This is not true in the case of inducers used in liquid rocket pumps. The blades of such inducers extend circumferentially over a major portion of a complete circle (fig. 1). Under

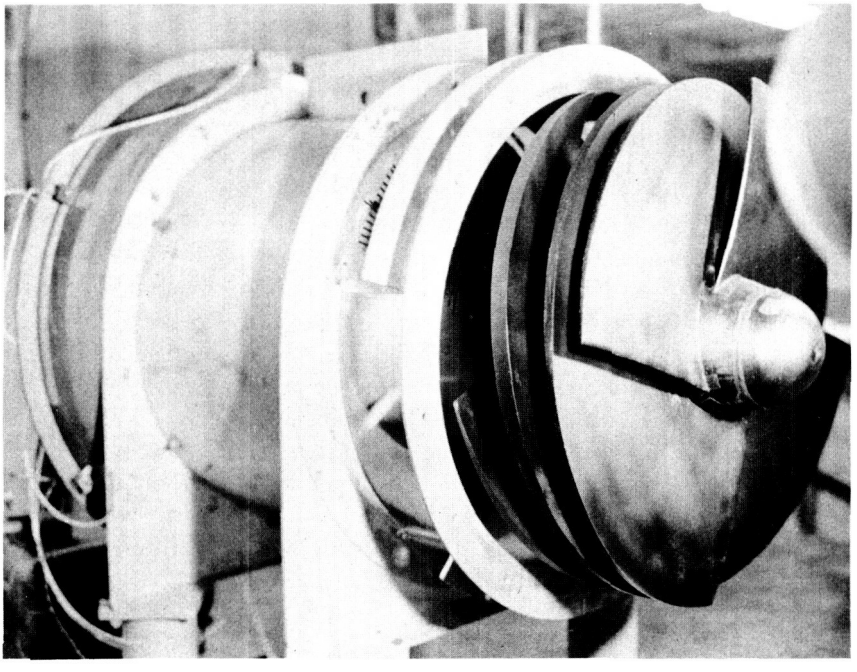

FIGURE 1.—*Photograph of the inducer (without shroud); 36-inch outside diameter, four blades.*

these circumstances, it can be estimated that the viscous effects and the consequent secondary motions are many times stronger than those encountered in other types of axial-flow machinery, and may indeed dominate the entire flow field. An understanding of such secondary motions is essential for the prediction of the efficiency and general performance of the inducer. The radial distribution of flow properties and the appropriate method of predicting them provide a further step toward the understanding of the flow through an inducer. This type of information is necessary for the analysis and design of the main pump. This is the objective of this paper.

The Department of Aerospace Engineering at The Pennsylvania State University has undertaken a systematic investigation with a view to understanding the general flow behavior and to developing flow prediction methods for inducers. A 3-foot-diameter inducer operated in air at a flow coefficient of 0.065 was built for this purpose. The following investigations, using the test rig shown in figure 2, have been completed so far:

(1) Visualization and measurement of the flow inside the passages[2] and at the exit of a four-bladed inducer. The latter measurements and an approximate analysis are reported in this paper.

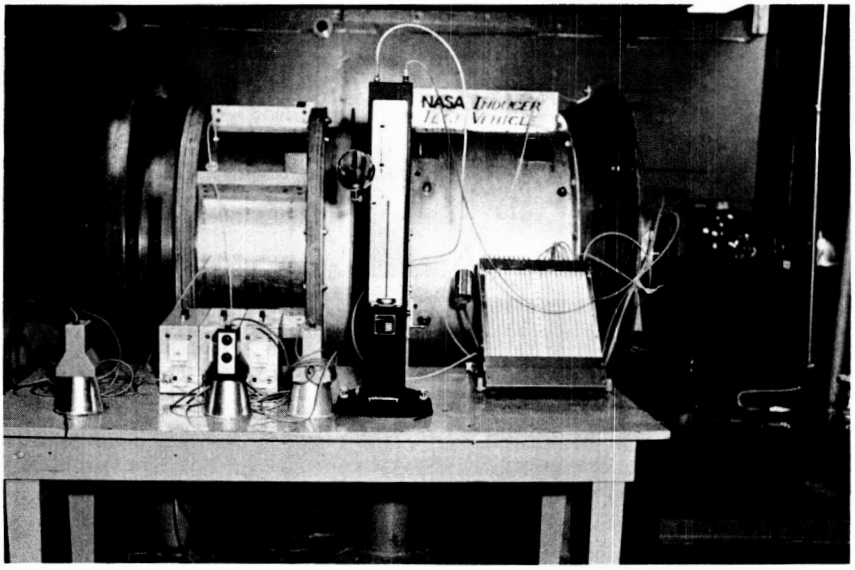

FIGURE 2.—*Test assembly.*

[2] These are carried out using rotating probes and pressure transfer device described in reference 20. The measurements are reported in reference 21.

(2) Three-dimensional velocity and turbulence measurements at the exit of a three-bladed inducer using hot-wire probes. Cooper and Bosch's computer program (ref. 9) is used to predict the three-dimensional inviscid effects (refs. 3 and 4).

(3) Three-dimensional turbulent boundary investigation on a single helical blade of the type used in rocket pump inducers (ref. 5).

These and future investigations to be undertaken will lead to the establishment of a theoretical model for the eventual analysis and design of turbomachinery flow dominated by secondary motions.

It is the intention of this paper to discuss the exit flow characteristics, a correlation for the frictional losses for the inducers, and an approximate analysis for the predictions of the velocity and energy distribution at the exit of the inducer. It will be shown that, while adequate information is not available to develop an exact analysis, the predictions based on loss correlations provide a method of predicting the gross behavior of the inducer.

DESIGN OF TEST INDUCER

The design of the test inducer is based on the "mean streamline" method developed by Wislicenus (ref. 6). The detailed design is described in reference 7. The overall characteristics are listed in table I.

After selecting a suction specific speed (SS) of 50 000 and head coefficient $\psi_T = 0.2$, the following parameters were derived from the design chart relating the cavitation parameters of turbomachines (fig. 259 in reference 6).

Flow coefficient, $\phi = 0.065$
Blade minimum pressure coefficient, $C_{P_{\min}} = 0.01$
$2gH_{sv}/V_z^2$

The runner is of free vortex design, producing constant head from root to tip. Using the relationship relating the stagnation head coefficient to change in tangential velocities, the inlet and outlet velocity diagrams are derived (fig. 3). The resulting runner profile is shown in figure 4. The design distribution of tangential and axial velocity components and of the stagnation and static head coefficients are shown in figures 11, 16, 18 and 20, respectively.

The design of blade sections is carried out in three steps:

(1) The mean streamline is derived from the assumed blade pressure diagram and blockage distribution as shown in figure 3. The blade pressure distribution chosen is typical of the trailing edge loaded profile which is required for this type of turbomachine and has $C_{P_{\min}} = 0.01$. In order to

account for the thickness or blockage effect of the blades, the relative velocities are varied from W_1 to W_2 along an arch-shaped curve above the nearly straight line variation that would apply to zero blade thickness. The arch-shaped curve represents an estimate of the blockage due to blade and boundary layer displacement thickness. The assumed blockage due to both effects is clearly marked in figure 3. The mean streamline for the hub and tip sections derived from the assumed pressure diagram and blockage is shown in figure 3.

(2) The departure of the camber line from the mean streamline is derived from the empirical deviation values of $\Delta\eta/L$ (nondimensionalized distance between the mean streamline and camber line measured normal to blade chord) derived by Wislicenus (ref. 6). It should be remarked here that Wislicenus' correlation for $\Delta\eta/L$ is the empirical counterpart of Ackeret's theoretical method (ref. 8). The validity of these empirical correlations for standard profiles has been established by Jakubowski (ref. 6) but its generalization to passages with nonstandard blade profiles

TABLE I.—*Inducer Characteristics*

Tip diameter		36.5 inches
Hub/tip ratio at outlet		0.5
Hub/tip ratio at inlet		0.25
Radial clearance		0.0625 inches
Suction specific speed SS (design)		50 000
Flow coefficient ($\phi = V_z/U_t$)		0.065
Blade chord	Tip ($R=1.0$)	82.96 inches
	Mid span ($R=0.75$)	63.18 inches
	Hub ($R=0.5$)	49.94 inches
Solidity	Tip ($R=1.0$)	2.86
	Mid span ($R=0.75$)	2.91
	Hub ($R=0.5$)	3.50
Number of vanes		4
Angular wrap (average)		290°
Lift coefficient of the blade based on mean velocity	Tip	0.0966
	Mid span	0.163
	Hub	0.307
Reynolds number based on tip radius		6.60×10^5
Reynolds number based on relative velocity and chord at mid radius		1.75×10^6
Maximum deviation of camber line from mean streamline $(\Delta\eta/L)_{max}$	($R=0.5$)	0.02
	($R=0.75$)	0.01075
	($R=1.0$)	0.00637
Blade angles at inlet	($R=0.25$)	75°30′
	($R=0.625$)	83°30′
	($R=1.0$)	86°15′

All other blade angles are given in figure 6.

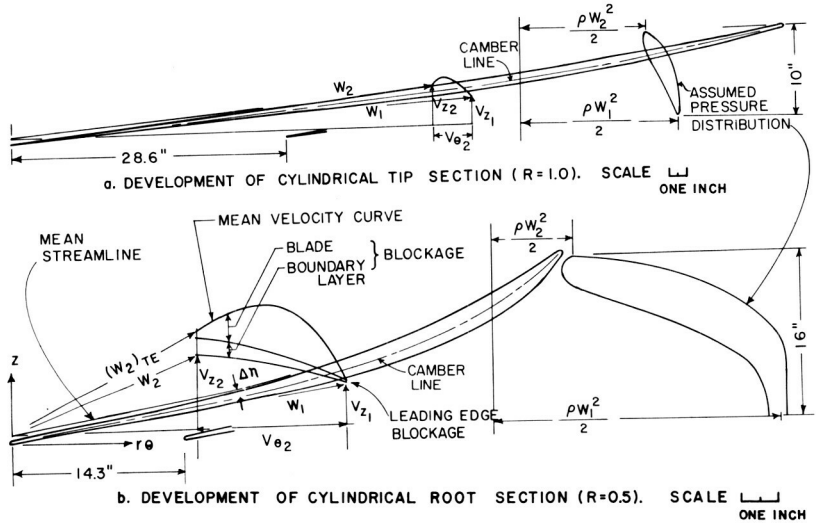

FIGURE 3.—*Design of blade profiles.*

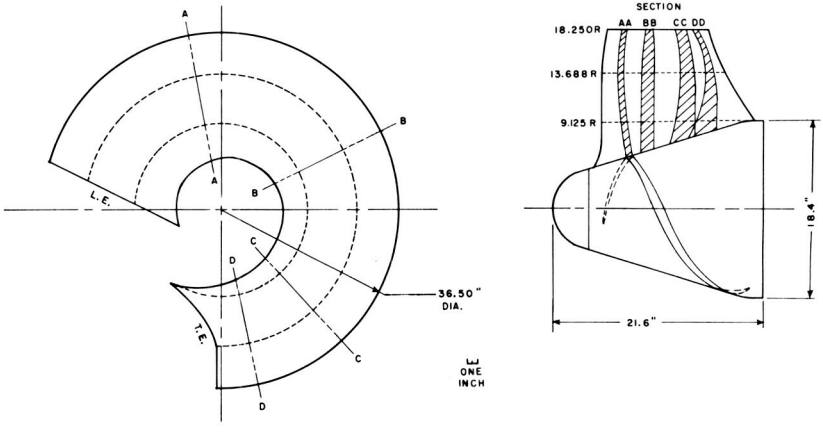

FIGURE 4.—*Axial view and circular projection of the inducer blade.*

and large stagger angle and solidities is yet to be established. The chordwise variation of $\Delta\eta/L$ assumed for this design departs from the NACA 65-series cascade data as required to obtain trailing edge loading (fig. 5). In figure 5, the notation $(\Delta\eta/L)_{\max,65}$ refers to the maximum deviation for a NACA 65-series cascade. Its value can be evaluated from the equation

$$\left(\frac{\Delta\eta}{L}\right)_{\max,65} = \left(\frac{\Delta\eta_1}{L}\right)_{\max} C_L$$

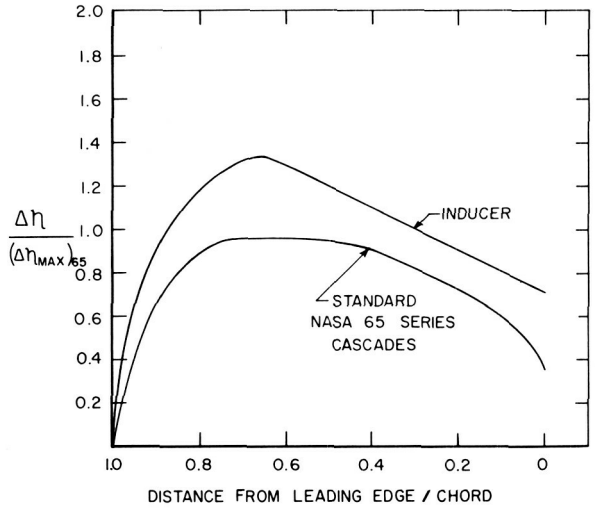

FIGURE 5.—*Assumed deviation of the camber line from the mean streamline.*

where

C_L lift coefficient

$\left(\frac{\Delta\eta_1}{L}\right)_{max}$ maximum deviation for unit lift coefficient

Their values for various vane chord angles are plotted by Wislicenus (fig. 298, ref. 6). The value of $(\Delta\eta_1/L)_{max}$ used for the inducer is 0.05 and the lift coefficients at various radial sections are given in table I. The camber lines so derived at hub and tip sections are shown in figure 3 and the design blade angles derived from this method are shown plotted in figure 6.

(3) The blade thickness can be derived from the assumed blockage curve (fig. 3) and the equation

$$\frac{\Delta V_z}{V_z}=\frac{t}{s}$$

where

ΔV_z perturbation in local axial velocity V_z due to blade blockage

t blade thickness in tangential direction

s blade spacing

The blade profiles so derived at hub and tip sections are shown plotted in figure 3.

FIGURE 6.—*Design blade and air angles.*

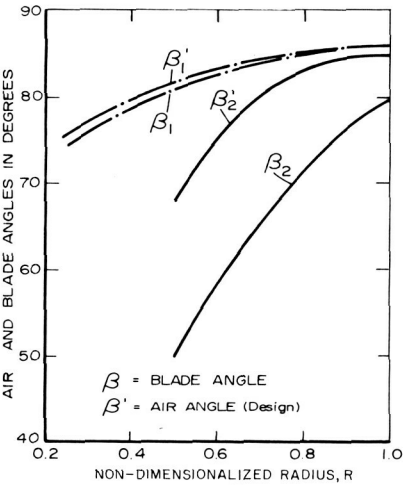

The blade section at hub ($R=0.5$), midradius ($R=0.75$) and tip sections ($R=1.0$) are designed in the manner explained above. The stacking of blade sections is carried out in much the same way as described by Wislicenus (ref. 6) and the final blade system so derived is shown in figure 4. In order to achieve reasonably constant variation in blade thickness from root to tip and smooth curvature in both chordwise and radial directions, it is sometimes necessary to change blade sections. This resulted in a slight departure from the free vortex design, especially at midradius, as shown in figures 20, 18, 16 and 11.

It should be remarked here that the Penn State inducer differs appreciably from the conventional radial blades of constant thickness (usually called flat plate inducer) used in practice. From the point of view of manufacture the radial blades are superior, but the design based on the present method should have hydrodynamically superior performance.

The blades for the inducer are of fiberglass construction, cast from suitable mold and templates. The final assembly of the test inducer, which is driven by a 5-hp variable-speed motor, is shown in figures 1 and 2. The research rotor is fitted with a pressure transfer unit which transmits pressures from a rotating blade to a stationary manometer.

APPROXIMATE THEORETICAL ANALYSIS

An attempt has been made to predict the flow properties at the exit of the inducer using a circumferentially averaged radial equilibrium equation. The three-dimensional nature of the flow and energy losses due to

friction are fully recognized in deriving the circumferentially averaged radial equilibrium equation for the inducer. The inducer passages are assumed to have fully developed turbulent flow. Based on the information available in the current literature, assumptions are made for the circumferential variation of the relative tangential and radial velocities. The frictional losses accounted for in the theory are based on a friction loss coefficient (analogous to the universal friction loss coefficient derived by Blasius for pipes) derived from various inducer tests carried out at NASA Lewis Research Center, TRW Cleveland, and M.I.T. Gas Turbine Laboratory. This friction loss coefficient, which takes into account rotational effects, is valid for low flow coefficient (upstream absolute velocity/blade tip speed) or high rotation parameter (blade tip speed/upstream absolute flow). The energy losses calculated from this newly derived friction loss coefficient are in close agreement with the energy loss measured in the Penn State inducer. The radial equilibrium equation derived in this section is valid for a noncavitating inducer.

The various assumptions made in deriving the radial equilibrium equation for the inducer are given in the text in proper context. The absolute and relative tangential velocities predicted from this equation are in good agreement with the measured values (see "Experimental Results and Discussion"). The velocity profile models used in this analysis are based on the three-dimensional boundary layer investigation carried out by Lakshminarayana et al. (ref. 5) for a single blade. The viscid effects are taken into account in an approximate manner by using an empirically derived loss coefficient in the final radial equilibrium equation. The analysis considers only the perturbations caused by viscous effects. The inviscid turning effects are allowed for by taking design or the potential flow solution as the boundary conditions for the solution of the radial equilibrium equation presented in this section.

No attempt has been made to predict the axial velocity components, which are very much smaller than the tangential velocity components. This prediction should await more accurate information on the three-dimensional nature of the flow in the rotating passages.

Equations of Motion

The equations of motion governing the incompressible and steady flow inside the passages in a coordinate system rotating with an angular velocity Ω (fig. 7) are given by reference 19,

$$\nabla I = 2\mathbf{W} \times \boldsymbol{\Omega} + \mathbf{W} \times (\nabla \times \mathbf{W}) + \mathbf{F} \tag{1}$$

$$\nabla \cdot \mathbf{W} = 0 \tag{2}$$

where

$$I=\frac{P}{\rho}+\frac{W^2}{2}-\frac{\Omega^2 r^2}{2} \tag{3}$$

and **F** is the frictional force per unit mass.

Since large velocity and pressure gradients exist in the case of an inducer, it is a formidable or impossible task to obtain an exact solution of equations (1) and (2). Hence, a more practical approach to satisfying the radial equilibrium equation on a circumferential average basis is employed in this paper. This technique was first employed by Ruden (ref. 10) for a compressor and later used by Smith (ref. 11) to derive a radial equilibrium equation amenable to solution by what is known as the "stream line curvature approach."

The scalar component of equation (1) in the radial direction is

$$\frac{\partial I}{\partial r}=-W_\theta\frac{\partial W_r}{r\partial\theta}-W_z\frac{\partial W_r}{\partial z}+W_\theta\frac{\partial W_\theta}{\partial r}+W_z\frac{\partial W_z}{\partial r}+\frac{W_\theta^2}{r}-2\Omega W_\theta+F_r \tag{4}$$

The following assumptions are made in deriving a radial equilibrium equation applicable to inducers operating at low flow coefficients.

(1) Frictional effects: The fluid friction affects the radial equilibrium equation through the terms F_r and I in equation (4). The radial component of shear stress at the blade surface is small, as indicated by Lakshminarayana's investigation (ref. 5) on a helical blade. It is recom-

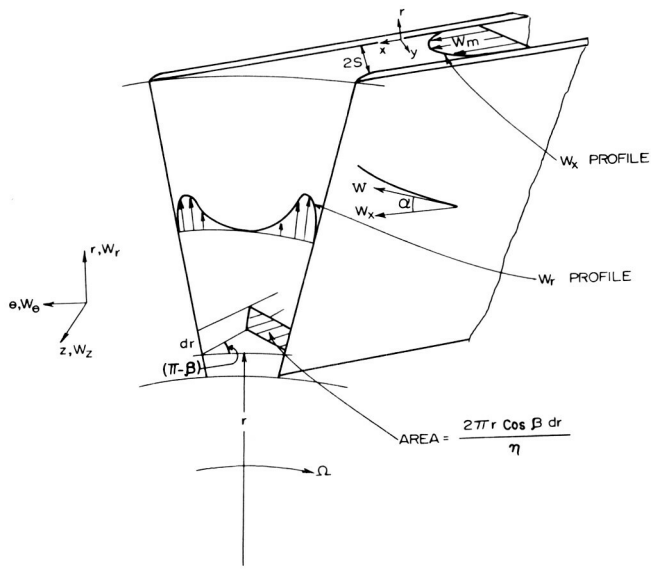

FIGURE 7.—*Notations used for inducer flow analysis.*

mended that the shear stress effect F_r be neglected in the preliminary analysis. In an inviscid flow, I is constant along a streamline. In viscid flow it can be approximated by

$$I=\frac{P}{\rho}+\frac{W^2}{2}-\frac{\Omega^2 r^2}{2}=C_1-\frac{\Delta P_0}{\rho}$$

where $\Delta P_0/\rho$ represents the stagnation pressure losses along a streamline. This term includes all losses associated with friction and turbulent mixing. In long, narrow inducer passages, this term is likely to be large. Thus,

$$\frac{\partial I}{\partial r}=-\frac{\partial}{\partial r}\left(\frac{\Delta P_0}{\rho}\right) \tag{5}$$

(2) For inducers operating at low flow coefficients,

$$\left.\begin{aligned} W_z &\ll W_\theta \\ \frac{\partial W_z}{\partial r} &\ll \frac{\partial W_\theta}{\partial r} \end{aligned}\right\} \tag{6}$$

(3) The flow passages are assumed to have fully developed flow and the flow properties are symmetrical about the midpassage (fig. 7). The assumptions for boundary velocity profiles are based on the investigations of reference 5 and are given by equations (12) and (13).

(4) The fluid is assumed to be guided smoothly through the channel (i.e., no flow deviation).

(5) The fluid is assumed to be single phase, incompressible and steady.

Assumptions (1) and (2) above would reduce equation (4) to

$$\underbrace{-W_\theta\frac{\partial W_r}{r\partial\theta}-W_z\frac{\partial W_r}{\partial z}+W_\theta\frac{\partial W_\theta}{\partial r}+\frac{W_\theta^2}{r}-2\Omega W_\theta}_{1\qquad 2\qquad 3\qquad 4}=\underbrace{-\frac{\partial}{\partial r}\left(\frac{\Delta P_0}{\rho}\right)}_{5} \tag{7}$$

Prior to deriving a circumferential average of the above equation, an attempt is made to present a method of evaluating the stagnation pressure loss (in relative flow) from inducer loss correlations.

Friction Loss Coefficient for a Rotating Channel with Large Rotation Parameter or Small Flow Coefficient

Since relative velocities are zero at the solid boundaries of a rotating channel, one is tempted to contemplate the behavior of the boundary layer in a frame of reference fixed to the rotor.

The fluid near the solid blade surfaces is not subjected to the same Coriolis or centrifugal forces as the main flow, and the result is that

externally impressed gradients produce secondary motions inside the blade boundary layer. The additional losses associated with these secondary motions increase the frictional losses. Investigations by Spannhake (ref. 13) and Ludweig (ref. 14) indicate that the loss coefficient in such rotating channels may be several times that of an equivalent[3] stationary channel. Very little is known about the increase in friction losses due to rotation, especially the additional frictional stresses induced by Coriolis force. Systematic experimental investigations by Spannhake (ref. 13) and Ludweig (ref. 14) indicate that these frictional losses are strongly dependent on the rotation parameter. This parameter is analogous to the Rossby number used in connection with studying the effect of earth rotation on wind profile and is defined as the ratio of Coriolis to inertia force.

Since very little analytical information is available for the type of rotating channel used in the inducer, a systematic attempt is made to correlate the measurements of various investigators to derive a friction factor for inducer channels for the range of rotation parameters (inverse of flow coefficient) used in practice. The inducer data collected are from various laboratories under different flow conditions and blade configurations. The frictional losses depend on Reynolds number, velocity, dimensions of the channel, rotation parameter, and aspect ratio of the blades. Since the available experimental data on inducers are meager and the tests involve a small range of Reynolds number, no systematic approach is used to find the Reynolds number dependency on losses. First, the Blasius friction factor (λ) is determined from the equation

$$\frac{\Delta P_0}{\rho} = \frac{\lambda}{2R_N{}^{1/4}} \frac{L}{d_h} \overline{W}^2 \tag{8}$$

where

$\Delta P_0/\rho$ is the loss in stagnation pressure of the relative flow
λ is the Blasius friction factor (0.316 for a stationary channel)
R_N is the Reynolds number, Wd_h/ν (fig. 7)
d_h is the hydraulic mean diameter (4 × area/wetted perimeter)
L is the length of the channel

For an elemental blade height dr of the inducer passage at any radius r (fig. 7)

$$d_h = \frac{4(2\pi r/n)\cos\beta\, dr}{2\, dr} = 4\frac{\pi r}{n}\cos\beta \tag{9}$$

where $\beta = f(r)$ and n is the number of passages.

---

[3] Equivalent here refers to a fully developed stationary channel having a mean velocity $\overline{W}$.

It is easy to prove that the nondimensionalized stagnation head loss coefficient in relative flow is equal to the difference between the Euler and measured head coefficient in absolute flow. Hence,

$$\psi_{\text{loss}} = \psi_E - \psi_m = \frac{2gH_{\text{loss}}}{U_t^2} = \frac{\lambda}{R_N^{1/4}} \frac{L}{d_h} \left(\frac{\overline{W}}{U_t} \right)^2 \tag{10}$$

where $H_{\text{loss}} = H_E - H_M$ is the head loss due to friction in relative flow.

For any given inducer, $\psi_E - \psi_m$ can be determined from the measured stagnation pressures and tangential velocities at the exit, and, knowing the inducer geometry, values of λ can be derived at any radii. The loss factor derived from various measurements carried out at NASA Lewis Research Center, M.I.T. Gas Turbine Laboratory, and TRW Cleveland are plotted in figure 8. The sources from which these data were collected and details of the inducer configurations and flow parameters used are given in table II. The radial distribution of Blasius loss coefficient showed a systematic trend from midradius to tip; i.e., an increase in frictional losses with decreasing flow coefficient. Dependency of energy losses on hub/tip ratio is also evident from figure 8. Larger secondary losses associated with low hub-tip ratios are well known. A new friction factor λ_R is defined and all the data are replotted to derive the value of this new friction factor.

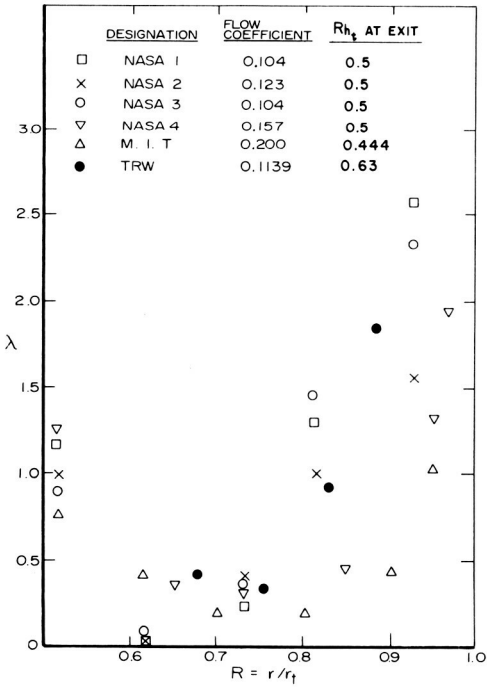

FIGURE 8.—*Radial variation of Blausius friction coefficient* (λ) *evaluated from equation* (10) *for various inducer configurations* (*table II*).

TABLE II.—*Details of the Various Inducer Configurations and Flow Parameters Used in Deriving the Friction Factors* λ *and* λ_R *(Figures 8 and 9)*[1]

Designation	Source and figure number	Outside Diameter (in.)	Number of Blades	Chord Length at the tip (in.)	RPM	Flow Coefficient at inlet	R_{ht} at exit	Reynolds number $R_N = Wd_h/\nu$ at mid radius
NASA 1	Reference 17 Figures 12f and 12h	5.0	3	12.25	15 000	0.107	0.5	2.24×10^6
NASA 2	Reference 17 Figures 12f and 12h	5.0	3	12.25	15 000	0.123	0.5	2.24×10^6
NASA 3	Reference 17 Figures 14f and 14h	5.0	3	12.25	7 500	0.104	0.5	1.12×10^6
NASA 4	Reference 18 Figures 14f and 14h	5.0	3	9.62	9 000	0.157	0.5	2.44×10^6
TRW	Reference 16 Figures 4.7.3–8	4.0	3	9.4	8 000	0.1139	0.63	1.72×10^6
M.I.T.	Reference 15 Figure 15	1.8	3	4.2	10 000	0.2000	0.444	3×10^5

[1] All inducers listed were tested in water.

$$\psi_{\text{loss}} = \frac{2gH_{\text{loss}}}{U_t^2} = \lambda_R \frac{R_{ht}}{\phi} \frac{1}{R_N^{1/4}} \frac{L}{d_h} \left(\frac{\overline{W}}{U_t}\right)^2 \tag{11}$$

where R_{ht} is the hub/tip ratio and $H_{\text{loss}} = \Delta P_0/\rho g$.

In these calculations, local values of blade length, hydraulic diameter, blade mean angle (arc tan $(\tan \beta_1 + \tan \beta_2)/2$), design flow coefficient, and measured local velocity (W) at the outlet are used to derive the new friction factor (λ_R) for the various inducer channels (fig. 9). It is not certain whether such a linear dependency on $\Omega r_t/W_z$ exists, but the data plotted in figure 9 seem to indicate that a relationship such as equation (11) is closely obeyed by all the inducer data plotted.

It should be remarked here that these loss correlations include mixing losses downstream of the trailing edge, since the measurements on which these loss correlations are based are taken for downstream of the inducer and not at the trailing edge.

It is suggested that a relationship such as the one discussed above be used with values of λ_R distribution shown in figure 9 for the flow coefficient ϕ ranging from 0.065 to 0.2. The largest scatter in the data is due to the M.I.T. inducer which was tested at $\phi = 0.2$. The secondary losses at the annulus and hub walls tend to be as important as secondary flow inside the blade boundary layer in such a case.

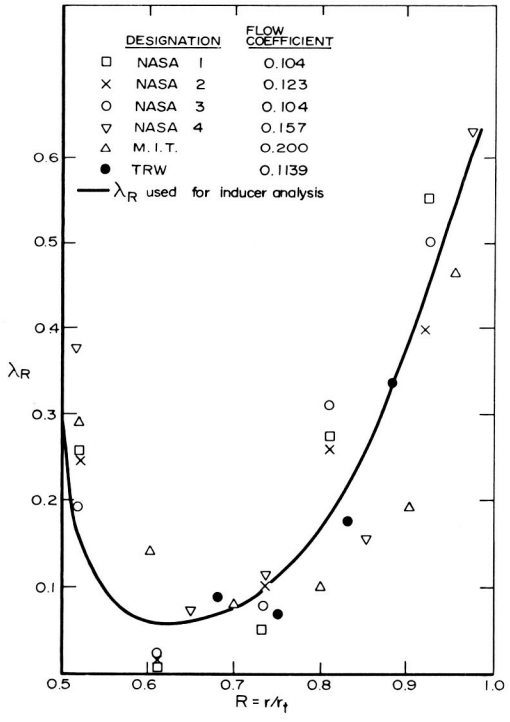

FIGURE 9.—*Radial variation of the modified friction loss coefficients* (λ_R) *calculated from equation (11) for various inducer configurations (table II).*

Circumferential Average of Radial Equilibrium Equation

The circumferential averaging of various terms in equation (7) is carried out under the following assumptions (fig. 7).

(1) The passages have fully developed turbulent flow and the flow properties are symmetrical about the midpassage.

(2) The velocity component parallel to the blade passage is given by

$$W_x = W_m \eta^{1/7} \tag{12}$$

where W_m is the velocity component parallel to the blade at midpassage, $\eta = y/S$, where y is the distance measured normal to the blade, $2S$ is the width of the channel (fig. 7) and x is the coordinate parallel to the blade and lying on a cylindrical surface.

(3) The radial velocity component W_r is given by reference 12,

$$W_r = W_x \tan \alpha (1-\eta)^2 = W_m \tan \alpha (\eta)^{1/7} (1-\eta)^2 \tag{13}$$

where α is the angle between the direction of the resultant velocity near the wall and W_m or angle between the limiting streamline and x direction (fig. 7). Note that W_m and α are functions of r and x only. The average of any quantity T will be denoted by a bar and is defined by

$$\overline{T} = \frac{1}{S} \int_0^s T \, dy \tag{14}$$

where $2S$ is the width of the blade passage.

Circumferential Average of Term 1 in Equation (7)

Since W_x is the velocity along x, where x is an intermediate variable and r, θ are the independent variables,

$$W_x \frac{\partial W_r}{\partial x} = W_z \frac{\partial W_r}{\partial z} + W_\theta \frac{\partial W_r}{r \partial \theta} \tag{15}$$

Now, from equation (13),

$$\frac{\partial W_r}{\partial x} = \eta^{1/7} (1-\eta)^2 \left(\frac{\partial W_m}{\partial x} \tan \alpha + W_m \sec^2 \alpha \frac{\partial \alpha}{\partial x} \right) \tag{16}$$

Hence, the circumferential average of Term 1 in equation (7) is

$$\overline{\frac{W_\theta}{r} \frac{\partial W_r}{\partial \theta} + W_z \frac{\partial W_r}{\partial z}} = \overline{W_x \frac{\partial W_r}{\partial x}}$$

$$= W_m \left(\frac{\partial W_m}{\partial x} \tan \alpha + W_m \sec^2 \alpha \frac{\partial \alpha}{\partial x} \right) \int_0^1 \eta^{2/7} (1-\eta)^2 \, d\eta$$

$$=0.210W_m\left(\frac{\partial W_m}{\partial x}\tan\alpha+W_m\sec^2\alpha\frac{\partial\alpha}{\partial x}\right) \tag{17}$$

Circumferential Average of Terms 2, 3, and 4 in Equation (7)

Since it is assumed that the fluid is smoothly guided through the passage, the circumferential average of Term 2 in equation (7) is

$$\overline{W_\theta\frac{\partial W_\theta}{\partial r}}=\int_0^1(W_\theta)_m(\eta)^{1/7}(\eta)^{1/7}\frac{\partial(W_\theta)_m}{\partial r}d\eta=1.015\overline{W_\theta}\frac{\partial\overline{W_\theta}}{\partial r} \tag{18}$$

since $\overline{W_\theta}=\frac{7}{8}(\overline{W_\theta})_m$ for one-seventh profile.

Similarly,

$$\overline{W_\theta{}^2}=\int_0^1 W_\theta{}^2\,d\eta=(W_\theta)_m{}^2\int_0^1\eta^{2/7}\,d\eta=1.015\overline{W_\theta}^2 \tag{19}$$

and

$$2\Omega\overline{W_\theta}=2\Omega\overline{W_\theta} \tag{20}$$

Circumferential Average and Radial Variation of the Frictional Losses in Equation (7)

Since the friction losses derived by the author (eq. 11) represent the average losses across the passage, the circumferential average of the fifth term in equation (7) is

$$\frac{\partial}{\partial r}\left(\frac{\Delta P_0}{\rho}\right)=\frac{\partial}{\partial r}\left(\lambda_R\frac{R_{ht}}{\phi}\frac{1}{R_N{}^{1/4}}\frac{L}{d_h}\frac{\overline{W}^2}{2}\right) \tag{21}$$

Hence, the circumferential average of the radial equilibrium equation now reads, after substituting equations (17), (18), (19), (20), and (21) in equation (7),

$$-0.210W_m\left(\tan\alpha\frac{\partial W_m}{\partial x}+W_m\sec^2\alpha\frac{\partial\alpha}{\partial x}\right)+1.015\overline{W_\theta}\frac{\partial\overline{W_\theta}}{\partial r}+1.015\frac{\overline{W_\theta}^2}{r}$$

$$-2\Omega\overline{W_\theta}+\frac{\partial}{\partial r}\left(\frac{\lambda_R}{R_N{}^{1/4}}\frac{R_{ht}}{\phi}\frac{L}{d_h}\frac{\overline{W}^2}{2}\right)=0 \tag{22}$$

Since $\overline{W_\theta}=\frac{7}{8}(W_\theta)_m=\frac{7}{8}W_m\sin\beta$, the final circumferentially averaged radial equilibrium equation valid for inducers operating at low flow coefficient is

$$\frac{-0.275}{\sin^2\beta}\overline{W_\theta}\left(\tan\alpha\frac{\partial\overline{W_\theta}}{\partial x}+\overline{W_\theta}\sec^2\alpha\frac{\partial\alpha}{\partial x}\right)+1.015\overline{W_\theta}\frac{\partial\overline{W_\theta}}{\partial r}$$

$$+1.015\frac{\overline{W_\theta}^2}{r}-2\Omega\overline{W_\theta}+\frac{\partial}{\partial r}\left(\frac{\lambda_R}{R_N{}^{1/4}}\frac{R_{ht}}{\phi}\frac{L}{d_h}\frac{\overline{W}^2}{2}\right)=0 \tag{23}$$

The solution of this circumferentially averaged radial equilibrium equation to derive $\overline{W_\theta}$ or $\overline{V_\theta}$ distribution along the radius is still intractable unless suitable assumptions are made for $\partial \overline{W_\theta}/\partial x$ and α. The experiment is the only source from which the values of α can be derived. The limiting streamline angle α is predictable in the case of a single rotating helical blade (ref. 5), but the values of α measured on inducer blade surfaces are found to be higher than those on a single helical blade (refs. 21 and 24). The evaluation of $\partial \overline{W_\theta}/\partial x$ could be based on either a linear variation of $\overline{W_\theta}$ along x or the inviscid solution. Once these quantities are evaluated, $\overline{W_\theta}$ or $\overline{V_\theta}$ can be predicted from equation (23) using the author's correlation for friction loss coefficient λ_R (fig. 9).

The method of predicting $\overline{W_\theta}$ or $\overline{V_\theta}$ for any given inducer geometry and flow coefficient is described in the next section.

EXPERIMENTAL RESULTS AND DISCUSSION

The four-bladed inducer described in the section on the design of the test inducer is used for the experimental investigations of the flow characteristics. The test medium is air and all the measurements are carried out at a Reynolds number (based on tip radius) of 6.6×10^5, which corresponds to 450 rpm. A throttle valve, which can be seen in figure 2, is adjusted to obtain a flow coefficient ϕ of 0.065.

The measuring stations are shown in figure 10. The exit flows were measured at stations 3, 4, 5, 6, and 7, using a stagnation probe and a tuft probe. Hot wire measurements were taken very close to the trailing edge (station 3A) to derive the average values of radial, axial, and tangential velocity components.

The outlet air angles (of the absolute flow) were measured by means of a very thin tuft probe and a sighting scope of the type used by Smith (ref. 22). Fluctuations in absolute air angles were found to be considerable, especially near the hub locations. The algebraic mean of the maximum and minimum air angles, measured by the tuft probe, was used for calculating the axial and tangential velocity components. In spite of slight inaccuracies which are discussed by McCafferty (ref. 20), much information can be gained from these stationary probe measurements. Since the flow at the exit was highly three-dimensional, the static pressures were measured at the hub and annulus walls and the radial distribution of static pressure coefficient was derived by computing the pressure gradient near the wall locations from the simplified radial equilibrium equation.

Since an accurate knowledge of the nature and magnitude of radial velocities is essential for the development of an adequate theory for predicting the flow, an attempt was made to derive the average values of all three velocity components at the exit (station 3A) using a combination

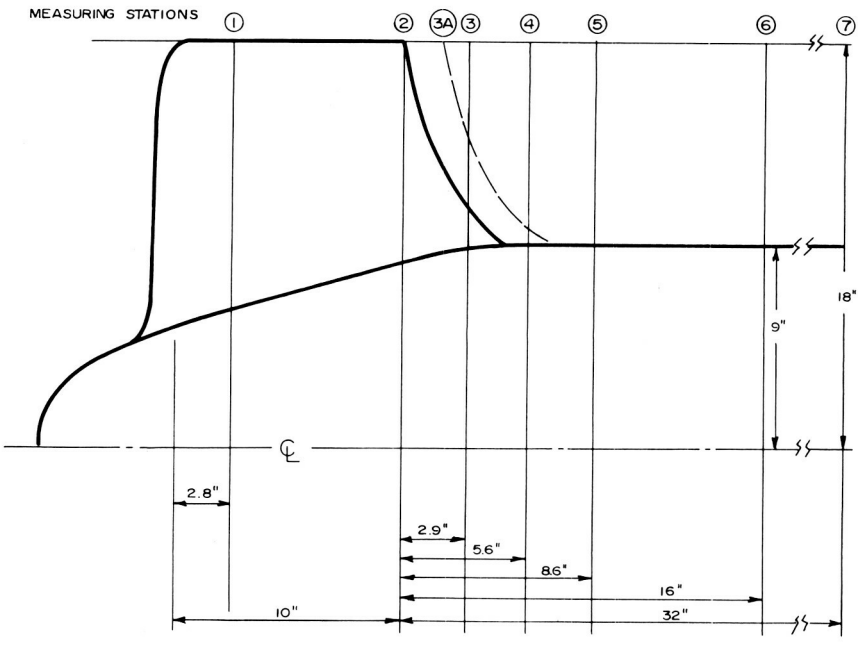

FIGURE 10.—*Location of the flow-measuring stations.*

of an X-configuration hot-wire probe plus a single sensor probe normal to the X-configuration. The probes were aligned in the three coordinate directions such that they sense the following velocity components.

$$V_{\theta z} = \sqrt{V_\theta^2 + V_z^2} \tag{24}$$

$$V_{\theta r} = \sqrt{V_\theta^2 + V_r^2} \tag{25}$$

$$V_{rz} = \sqrt{V_r^2 + V_z^2 + K^2 V_\theta^2} \tag{26}$$

Since the air angles of the absolute flow are very large, a correction to the cosine law was used for the wire in the θ direction. This appears in the form of a correction factor as shown in equation (26). The value of K was derived from Schwarz and Friehe's correlations (ref. 23). For the length/diameter of the wire used in these experiments, the value of K was found to be 0.26.

The oscilloscope traces of the signal were photographed[4] to derive the blade-to-blade variation of the voltages. The hot-wire calibration curves and equations (24), (25), and (26) were then used to derive the blade-to-blade variation of V_r, V_θ, and V_z.

[4] The method of data processing has since been improved as indicated in reference 4.

Tangential Velocities at Exit

The absolute tangential velocities derived from pressure and angle measurements are shown plotted in figure 11 for various axial stations. The measured tangential velocities are substantially higher than the design values except near the hub. These results are consistent with the measurements reported by Sandercock et al. (ref. 17) and Soltis et al. (ref. 18). The real fluid effects combined with large radial flows that exist inside the blade passages are responsible for such a large increase in tangential velocity or head rise. Furthermore, it is also evident from figure 11 that there is a substantial change in tangential momentum as the flow proceeds downstream. Far downstream of the inducer, a "forced vortex" type of distribution exists. Such changes are due to mass flow redistribution that takes place downstream of the inducer and the mixing losses due to blade wake diffusion. The extent of mass flow redistribution can be seen from figure 16. These measurements indicate the desirability of having the inducer as an integral part of the main pump and also point out the need to take measurements close to the trailing edge in order to accurately assess the extent of real fluid effects inside the blade passages. It is quite clear that the inducer behaves like a drag or a friction pump, especially near the tip, where the head rise is imparted to the fluid by purely frictional effects.

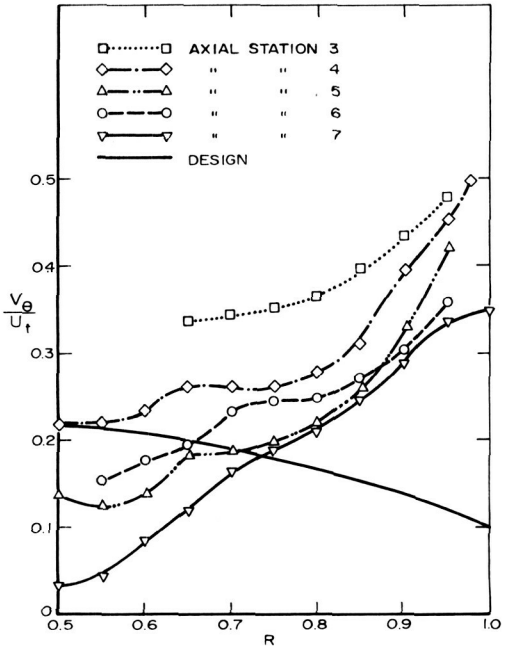

FIGURE 11.—*Radial variation of absolute tangential velocity at various axial locations.*

Even though an accurate prediction of the tangential velocity distribution is possible only by a thorough understanding of the three-dimensional boundary layer characteristics inside the passage, a qualitative estimate of the frictional effects can be made from an analysis of the type indicated in the preceding section (Approximate Theoretical Analysis).

The form of equation used for predicting the tangential velocities at the exit of the inducer is obtained by further simplification of equation (23) (by expressing $\overline{W_\theta}$ as the only dependent variable) under the following assumptions:

(1) $\overline{W_\theta}$ varies linearly with x from leading to trailing edge.

(2) Angle α between the limiting streamline and W_m varies linearly from leading edge to trailing edge, being zero at the leading edge. This trend is confirmed from the limiting streamline angle measurements reported in reference 21. Hence,

$$\frac{\partial W_\theta}{\partial x} = \frac{\overline{W_\theta} - \Omega r}{L} = \frac{\overline{W_\theta} - \Omega r}{4.5r} \tag{27}$$

where

$\overline{W_\theta}$ = relative tangential velocity at exit

$\Omega r \cong$ relative tangential velocity at inlet

L = chord length of the blade ($\cong 4.5r$ for Penn State inducer)

and

$$\frac{\partial \alpha}{\partial x} = \frac{\alpha - 0}{4.5r} \tag{28}$$

where α is the angle of the limiting streamline near the trailing edge. Use of equations (27) and (28) would reduce the first term in equation (23) to

$$\frac{-\overline{W_\theta}^2}{r} \zeta(r) + 2\overline{W_\theta}\Omega\xi(r) \tag{29}$$

where

$$\zeta(r) = \frac{0.061}{\sin^2 \beta} (\tan \alpha + \alpha \sec^2 \alpha) \tag{30}$$

$$\xi(r) = \frac{0.03 \tan \alpha}{\sin^2 \beta} \tag{31}$$

The friction loss term in equation (23) can be further simplified for the Penn State inducer to give

$$\frac{\partial}{\partial r}\left(\lambda_R \frac{R_{ht}}{\phi} \frac{1}{R_N{}^{1/4}} \frac{L}{d_h} \frac{\overline{W}^2}{2}\right) = \frac{\partial}{\partial r}\left(F(r\overline{W_\theta})^2\right)$$

$$= F'(r)\overline{W_\theta}^2 + 2F(r)\overline{W_\theta}\frac{\partial \overline{W_\theta}}{\partial r} \tag{32}$$

where

$$F(r) = \frac{1}{2} \frac{\lambda_R}{R_N{}^{1/4}} \frac{R_{ht}}{\phi} \frac{L}{d_h} \frac{1}{\sin^2 \beta} \tag{33}$$

and λ_R (fig. 9), $R_N{}^{1/4}$, d_h (eq. (9)), length of the blade (L), and $\sin^2 \beta$ (fig. 6) are all functions of radius at any given axial station. The variation of $F(r)$ with radius at the location of the trailing edge is plotted in figure 12. Hence, the final form of radial equilibrium equation used for predicting the relative tangential velocity at the exit of the Penn State inducer is obtained by substituting equations (29) and (32) in equation (23).

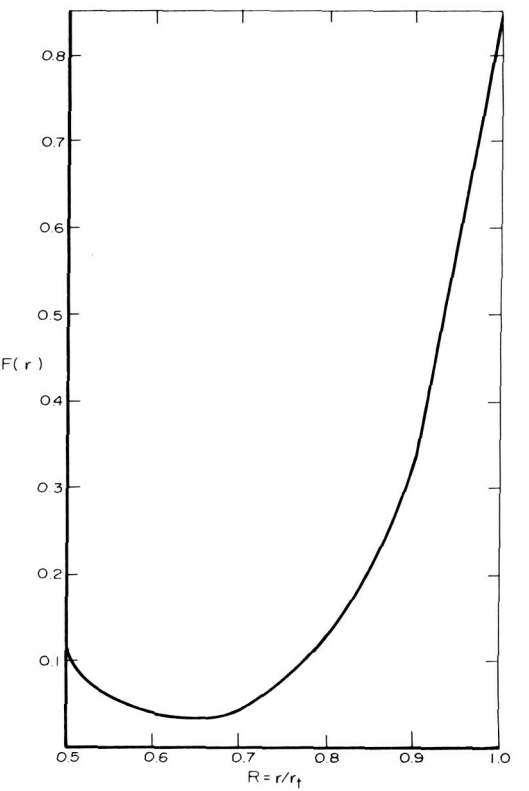

FIGURE 12.—*Radial variation of function* F(r) *(eq. (33)) for Penn State inducer.*

$$\overline{W_\theta}\frac{\partial \overline{W_\theta}}{\partial r}(1.015+2F(r))+\frac{\overline{W_\theta}^2}{r}(1.015+rF'(r)-\zeta(r))=2\Omega\overline{W_\theta}(1-\xi(r)) \tag{34}$$

where the functions $F(r)$, $\zeta(r)$, and $\xi(r)$ are defined by equations (33), (30), and (31), and $F'(r)$ is the derivative of $F(r)$ plotted in figure 12.

Equation (34) is used to predict the radial variation of mean relative tangential velocity ($\overline{W_\theta}$) at the trailing edge. In evaluating the functions $\zeta(r)$ and $\xi(r)$, information obtained by flow visualization experiments reported in reference 24 is used. Near the hub, the value of α was found to be nearly 60° on the suction surface and 30° on the pressure surface of the blade. Basing our assumption on this, α is assumed to vary linearly from 45° at the hub to zero at the tip (fig. 13). This enabled evaluation of the functions $\zeta(r)$ and $\xi(r)$ (eqs. (30) and (31)) in equation (34). The variations of these functions with radii are plotted in figure 13.

The predicted values of relative tangential velocity at the trailing edge obtained from equation (34), using estimated values of $F(r)$, $F'(r)$, $\zeta(r)$, and $\xi(r)$ (figs. 12 and 13), are plotted in figure 14. The boundary condition assumed for the solution of the differential equation (34) is that the tangential velocity ($\overline{W_\theta}$) at the midradius is the same as that of design. The predicted values are in good agreement with the values derived from stationary probe measurements at station 5.[5]

The effect of neglecting the inertial terms due to radial velocity gradients (i.e., functions $\zeta(r)$ and $\xi(r)$ in equation (34)) is also shown in figure 14. The inertial terms due to radial velocity gradients in the radial equilibrium equation seem to have very little effect on the predicted values of $\overline{W_\theta}$. Even though the acceleration components due to radial velocity gradients are small, their influence in increasing the frictional losses cannot be ignored. Hence, in conclusion, it can be said that the acceleration component due to radial velocity gradients can easily be neglected in predicting the relative tangential velocity distribution from the radial equilibrium equation. But the influence of radial velocities on axial velocity profile at the exit cannot be ignored.

In deriving equation (34) from the generalized radial equilibrium equation (eq. (4)), it was assumed that the term $W_z(\partial W_z/\partial r)$ is very small. Its influence on the predicted values of $\overline{W_\theta}$ is evaluated by using the

---

[5] It should be remarked here that the loss coefficient (λ_R) derived in this paper is based on the measurements carried out at one-seventh to one-ninth blade chord (refs. 15, 17, and 18) downstream of the trailing edge. Hence, these loss correlations include mixing losses. To be consistent, only the measurements carried out at station 5, which approximately corresponds to the measuring stations of references 15, 17, and 18, is compared with the predicted values.

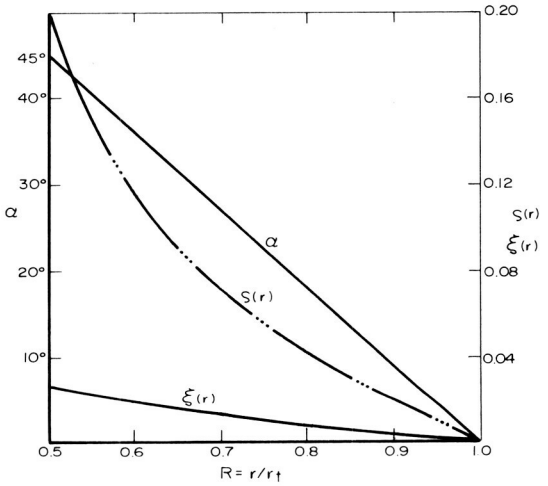

FIGURE 13.—*Radial variation of* ζ(r) *and* ξ(r) *(eqs. (30) and (31)) and assumed* α.

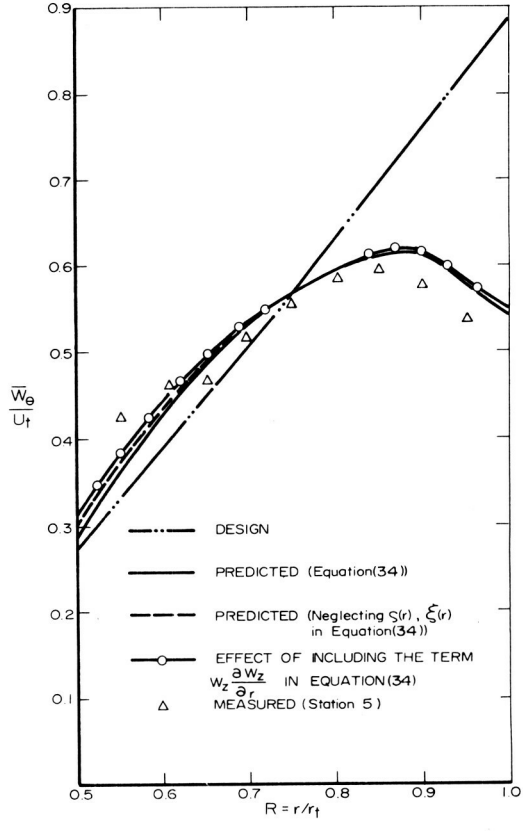

FIGURE 14.—*Predicted and measured relative tangential velocity.*

experimental values of $W_z(\partial W_z/\partial r)$ (fig. 16) and the following modified equation

$$\overline{W_\theta}\frac{\partial \overline{W_\theta}}{\partial r}(1.015+2F(r))+\frac{\overline{W_\theta}^2}{r}(1.015+rF'(r)-\zeta(r))+\overline{W_z}\frac{\partial \overline{W_z}}{\partial r}$$
$$=2\Omega\overline{W_\theta}(1-\xi(r)) \quad (35)$$

The effect of neglecting the axial velocity gradient term in equation (34) is evident from figure 14. The effect of this term on the predicted values of $\overline{W_\theta}$ seems to be appreciable only near the hub (where the axial velocity gradients are large) and negligibly small at other radial positions.

The predicted tangential velocity components of the absolute flow $(U-\overline{W_\theta})$ are plotted and compared with experimental values, derived from stationary probe measurements[6] at station 5, in figure 15. The agreement between the predicted and experimental values is good. The inclusion of the axial velocity gradient term $W_z(\partial W_z/\partial r)$ in equation (34) seems to bring the predicted values of $\overline{V_\theta}$ closer to the experimental values only near the hub.

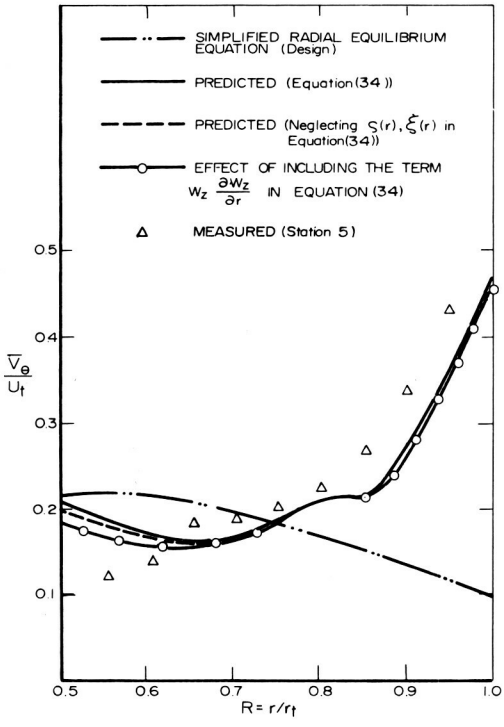

FIGURE 15.—*Predicted and measured values of absolute tangential velocity.*

[6] See footnote 5.

The effect of neglecting the radial velocity gradients $\zeta(r)$ and $\xi(r)$ in equation (34) is shown in figure 15. It is evident that the friction loss term in the radial equilibrium equation (eq. (7)) has a very appreciable effect in changing the tangential velocity gradient in the radial direction.

The tangential velocity distribution derived from hot-wire probe and stationary probe measurements, carried out very close to the trailing edge (station 3A), is compared in figure 17. There is a slight discrepancy between the two measurements. This may be due to error in measuring the fluctuating (with reference to stationary probe) stagnation pressure close to the trailing edge.

Axial Velocities at the Exit

The measured radial distribution of axial velocities at various axial stations is plotted in figure 16.

Immediately downstream of the inducer (stations 3 and 4), the minimum velocity occurs at the midradius. This seems to suggest that radial migration inside the blade boundary layer is very large from midradius to tip as compared to that from hub to midradius. At station 3, where the hub flow is still under the influence of blade, the blockage effects are large. Sandercock et al. (ref. 17) and Soltis et al. (ref. 18) concluded earlier that the inducers operating at low flow coefficients have separated flow near the hub. These conclusions are based on measurements taken far downstream. The present investigation seems to suggest that such flow separation takes place downstream of the inducer due to considerable flow redistribution. It should be remarked here that large radial velocities exist

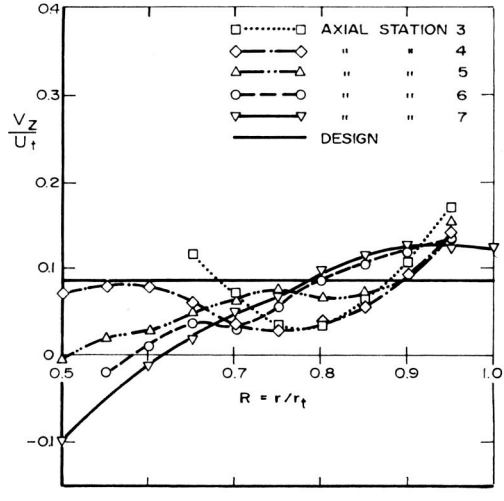

FIGURE 16.—*Radial variation of axial velocity at various axial locations.*

in the blade wakes of the inducer. This accounts for large changes in axial and tangential velocities and stagnation pressures measured downstream (figs. 11, 16, and 18).

Far downstream of the inducer (stations 5, 6, and 7), the minimum axial velocity occurs near the hub, and in fact shows a tendency to separate at station 5. Downstream of the inducer, the radial velocities inside the blade wakes are outward near the hub, whereas the wake interactions near the tip produce an inward flow. The net effect is a migration of the mass flow toward the midradius. This effect can be clearly seen at stations 5 and 6. Thus, there is a substantial improvement in axial velocity distribution near the midradius and a deterioration near the hub. Furthermore, the extent of back flow is observed to grow continuously as the flow proceeds downstream and occupies nearly 20 percent of the annulus far downstream (station 7, fig. 16). In a pumping unit where the inducer is an integral part of the main pump, the back flow may be absent if aerodynamically designed blade sections are used. It is not clear whether this is true for flat plate inducers, since measurements close to the trailing edge are not available for such units. Inside the blade passages, the perturbation in axial velocity is due to:

(1) Radially varying blade thickness and hence blockage

(2) Radial flow inside the blade boundary layers. This is by far the most important cause of the change in axial velocities from hub to tip.

The perturbations in downstream flow are predominantly due to radial velocities in the three-dimensional wakes.

The prediction of axial velocity distribution should take into consideration the detail flow structure, including the radial velocities inside blade boundary layers, inside such inducers. The boundary layer in a rotating helical channel, currently under investigation at Pennsylvania State University, should provide the urgently needed information for the accurate prediction of axial velocity distribution. Thus, considerably more theoretical and experimental work is necessary before the observed flow can be regarded as rationally explained.

It should be emphasized here that the flow redistribution downstream of the inducer (caused by the radial velocities in the three-dimensional blade wakes) is considerable and extreme caution should be exercised in evaluating the performance of an inducer from the measurements obtained far downstream.

The average values of the axial velocities derived from the hot-wire probe measurements very close to the trailing edge are shown plotted and compared with stationary probe measurements in figure 17. This seems to confirm the trend in axial velocity discussed earlier; i.e., very low axial velocities at midradius.

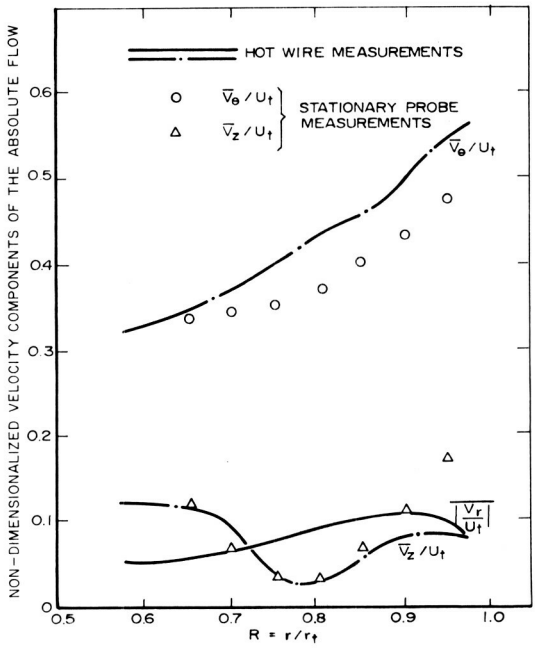

FIGURE 17.—*Comparison of the absolute velocity components measured by the hot wire and stationary probe at station 3A.*

Radial Velocities at Exit

The radial distribution of average radial velocities ($\overline{|V_r|}$) derived from the hot-wire measurements is plotted in figure 17.[7]

It should be remarked here that the hot-wire probe senses only the magnitude and not the direction of the radial velocity. Near the inducer tip, radial *inward* flow exists due to boundary layer interactions. Thus, the algebraic average of radial velocities across the passage is likely to be different from $\overline{|V_r|}$, especially near the tip.

It is evident from figure 17 that the radial velocities are of the same order of magnitude as axial velocities, with values increasing monotonically toward the tip. The maximum average radial velocity occurs a small distance away from the tip (fig. 17) and this location corresponds to the maximum inward flow region.

These measurements confirm the earlier conclusion that radial velocities in such low flow coefficient and high solidity inducers are large. For the eventual flow analysis, it is essential to know the detail blade-to-blade variation of radial velocities including the extent of radial inward flow.

---

[7] Discrepancy between the hot-wire results reported in reference 21 (unpublished) and this paper is due to the fact that earlier results are based on $K=0$ in equation (26).

Stagnation Pressure Coefficient at Exit

The radial variation of stagnation head coefficient at various axial stations is shown plotted in figure 18 and compared with design values. These plots are typical of inducers tested earlier (refs. 17 and 18). The pressure coefficients near the tip are two to three times the corresponding design values. Strong real fluid effects from midradius to tip are thus evident. The performance of the inducer is similar to a "shear force pump" or "drag pump," where shear forces are utilized to exchange kinetic energy between fluid and solid bodies. Thus, the sections near the tip operate predominantly as a shear force pump, whereas the pressure rise near the hub is largely due to flow turning effects.

The stagnation head decreases continuously as the flow proceeds downstream of the trailing edge. Major changes occur between stations 3 and 4, especially near the hub. Comparing the corresponding axial velocities at stations 3 and 4 in figure 16, it is evident that the major effects come from the axial velocity changes. The wake mixing losses also contribute to the change in stagnation head. These effects are dominant from midradius to tip. The tip sections experience considerable pressure losses as the flow proceeds downstream despite the fact that axial velocity changes (fig. 16) are small. The presence of large mixing losses is thus evident in these regions.

An attempt is made to estimate the stagnation pressure or head rise coefficient and losses on the basis of the analysis indicated in the preceding section (Approximate Theoretical Analysis). The knowledge of the

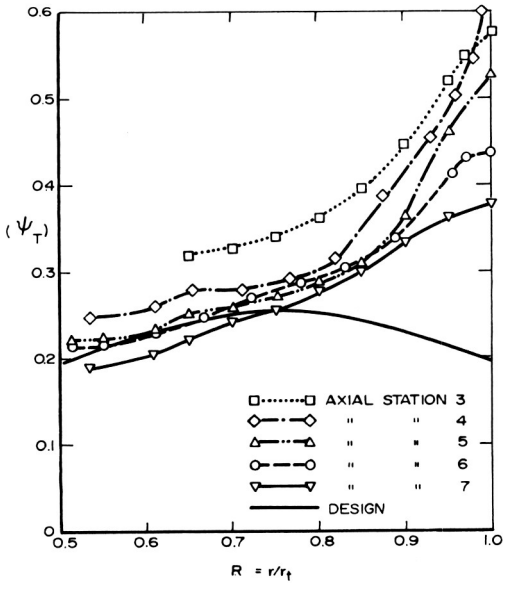

FIGURE 18.—*Radial variation of absolute stagnation pressure coefficient* (ψ_T) *at various axial locations.*

relative velocities derived from the theory outlined earlier (see Tangential Velocities at Exit and fig. 15) enables an estimate of the energy losses to be made from equation (11). The loss coefficients so derived are shown compared with the measured losses in figure 19 for station 5.[8] Reasonably good agreement between the estimated and measured losses confirms the validity of an empirical correlation such as equation (11) for estimating the energy losses associated with friction.

Since the theoretical values of Euler head ($\psi_E = 2RV_\theta/U_t$) are known from the predicted values of V_θ (fig. 14), the actual head rise can be estimated from the equation $\psi_T = \psi_E - \psi_{loss}$.

The value of ψ_T thus estimated is shown plotted and compared with measured values at station 5 in figure 19. Here again, the agreement is reasonably good and large gradients in stagnation head near the tip are estimated qualitatively.

Static Pressure Coefficient at the Exit

The static pressure coefficients derived at various axial locations are plotted and compared with design values in figure 20.

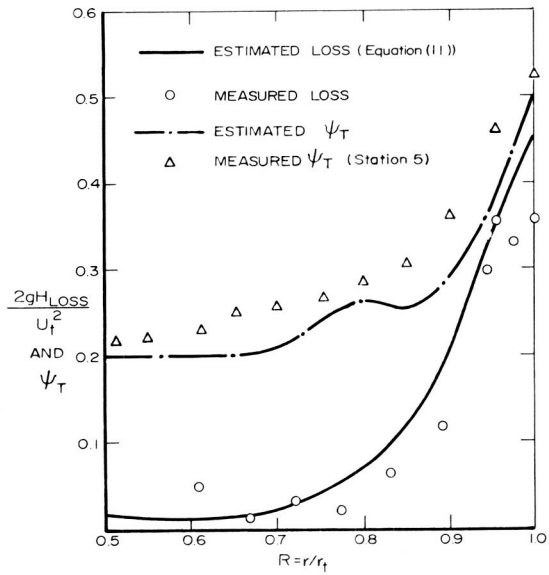

FIGURE 19.—*Estimated and measured friction losses and stagnation pressure coefficient* (ψ_T).

[8] See footnote 5.

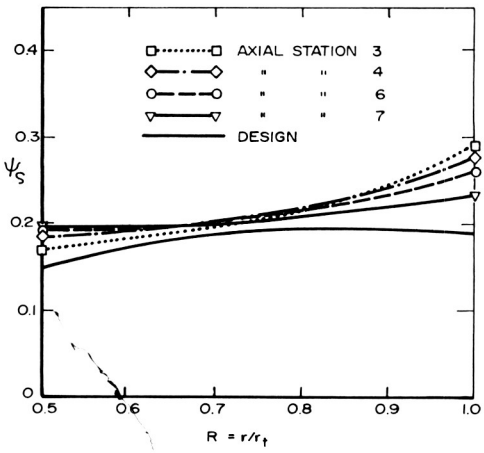

FIGURE 20.—*Radial variation of* ψ_S *at various axial locations.*

Near the tip, the measured pressure gradients are found to be large compared to those of the design. This is in conformity with the radial equilibrium requirements since tangential velocities at these locations are very large. It should be remarked here that the hub flow at station 3 is still under the influence of the rotor and hence the increase in ψ_S observed between stations 3 and 4. There is appreciable loss in static pressures as the flow proceeds downstream.

SUMMARY AND CONCLUSIONS

(1) A new friction loss coefficient applicable to inducers operating in the range of flow coefficients $\phi=0.065$ to $\phi=0.2$ is defined and derived from the inducer data available in the literature. This empirical friction loss coefficient is found to increase exponentially toward the blade tip. For the Penn State inducer, the radial variation of frictional losses estimated from this newly derived empirical loss coefficient agrees closely with the measured values.

(2) A circumferentially averaged radial equilibrium equation is used to predict the relative and absolute tangential velocities. The analysis is based on suitable assumptions for the radial and mainflow velocity profiles (based on the existing three-dimensional turbulent boundary layer data available) and the loss coefficients explained above. The agreement between theory and experiment is reasonably good. Hence it is evident that, if the frictional effects are known either empirically or analytically, the flow properties at the exit of the inducer can be predicted quite accurately. The stagnation head rise estimated from the predicted tangential velocities and the stagnation pressure losses (item (1)) agree qualitatively with the measured values.

(3) The test inducer, designed approximately for uniform head distribution over its discharge area (assuming ideal flow), actually produces a nonuniform head. Near the tip, the actual head of the absolute flow was found to be two to three times that at hub and midradius. This nonuniform head distribution can be explained qualitatively by real fluid effects and is in agreement with the observations of other investigators. The stagnation pressures are found to decrease continuously as the flow proceeds downstream. The wake mixing losses combined with large change in axial velocity distribution are the major causes of this.

(4) The expected radial motions within the blade passages have been qualitatively confirmed by hot-wire measurements and appear to be quite strong at all radii. The radial velocities are found to be of the same order of magnitude as axial velocities and increase continuously towards the tip.

(5) Measurements carried out several stations downstream indicate that the axial velocity profiles undergo marked changes as the flow proceeds downstream. The back flow region develops after the flow has left the rotating hub and grows continuously as the flow proceeds downstream. The minimum velocity occurs near the midradius, immediately downstream of the trailing edge, whereas, far downstream, the hub locations have minimum axial velocity.

(6) The absolute tangential velocities are substantially higher than the design values, except near the hub. These are consistent with the stagnation pressure rise observed. There is a large change in tangential velocities as the flow proceeds downstream. This is caused by mass flow redistribution and mixing losses that occur downstream of the inducer.

(7) The measured static pressure gradients are found to be large compared to those of design, especially near the tip. There is appreciable loss in static pressures in the tip flow as the flow proceeds downstream.

ACKNOWLEDGMENT

The author wishes to thank G. F. Wislicenus, who initiated this research and was largely responsible for the design of the test inducer. Acknowledgment is also made to several individuals who participated in various phases of the research program. Among these are C. A. Gorton, N. F. Wood, and C. E. Mothersbaugh.

LIST OF SYMBOLS

d_h	Hydraulic mean diameter (equation (9))
F	Frictional force per unit mass
$F(r), \zeta(r), \xi(r)$	Functions defined in equations (33), (30), and (31)

H	Stagnation head rise (in absolute flow)
H_E	Head rise derived from Euler's Equation (UV_θ/g)
H_{loss}	$H_E - H_m$
H_m	Measured stagnation head rise (in absolute flow)
H_{sv}	Net positive suction head, ft
h	Static head
L	Blade chord length
N	Rotative speed, rpm
n	Number of blades
P	Static pressure
P_0	Stagnation pressure
ΔP_0	Stagnation pressure loss due to friction
Q	Flow rate, gpm
R	r/r_t
R_{ht}	Hub/tip ratio
R_N	Reynolds number, $\overline{W}\, d_h/\nu$
r, θ, z	Radial, tangential, and axial coordinates
$2S$	Width of the passage measured normal to blade surface
SS	Suction specific speed, $N\sqrt{Q}/H_{sv}^{3/4}$
s	Blade spacing
U	Blade speed
V	Resultant absolute velocity
W	Resultant relative velocity
x, y	Coordinates parallel to and perpendicular to blade camber line and lying on a cylindrical surface (fig. 7)
α	Angle between limiting streamline and x direction (fig. 7)
β	Blade angle measured from axial direction
β'	Air angle measured from axial direction
η	y/S
$\Delta\eta$	Distance between the mean streamline and camber line normal to blade chord
λ	Blasius friction coefficient defined in equation (8)
λ_R	Friction coefficient for a rotating channel defined by equation (11)
ν	Kinematic viscosity
ρ	Density
ϕ	Flow coefficient, $W_z/\Omega r_t$
ψ_E	$2gH_E/U_t^2$
ψ_{loss}	$2gH_{\text{loss}}/U_t^2$
ψ_S	$2gh/U_t^2$ (static head rise coefficient)
Ω	Angular velocity
ψ_T	Stagnation head coefficient, $2gH/U_t^2$

Subscripts

h	Hub
m	Values at midpassage
RMS	Root-mean-square value
r, θ, z	Components along r, θ, z directions
t	Tip
x, y	Components along x, y directions (fig. 7)
1	Inlet
2	Outlet

Superscript

$-$	Averaged over the passage

REFERENCES

1. Acosta, A. J., An Experimental Study of Cavitating Inducers. *Proc. Second Symposium on Naval Hydrodynamics* (Washington, D.C.), August 25, 1958.
2. Arcand, L., *The Performance of Two Axial Flow Water Jet Pumps.* ASME Symposium on Pumping Machinery for Marine Propulsion, May 1968.
3. Poncet, A., and B. Lakshminarayana, *Investigations and Analysis of Flow Phenomona in Axial Flow Inducers.* NASA CR 107267, October 1969.
4. Poncet, A., and B. Lakshminarayana, *Investigations of Three-Dimensional Flow Characteristics in a Three Bladed Rocket Pump Inducer.* NASA CR-2290, 1973.
5. Lakshminarayana, B., A. Jabbari, and H. Yamaoka, Turbulent Boundary Layer on a Rotating Helical Blade. *J. Fluid Mech.*, Vol. 51, p. 547, 1972.
6. Wislicenus, G. F., *Fluid Mechanics of Turbomachinery.* Dover, Inc., 1965, Chapter 29.
7. Wislicenus, G. F., and B. Lakshminarayana, *Design of a Test Inducer.* Progress Report, NASA Contract NSG 537, March 1964.
8. Ackeret, Contribution to the Layout of Closely Spaced Cascade of Vanes. *Schweizer Bauzeitung*, Vol. 120, No. 9, August 1942.
9. Cooper, P., and H. Bosch, *Three-Dimensional Analysis of Inducer Fluid Flow.* NASA CR 54836, TRW ER 6673A, February 1966.
10. Ruden, P., *Investigations of Single-Stage Fans.* NACA TM 1062, April 1944.
11. Smith, L. H., The Radial Equilibrium Equation of Turbomachinery. *Trans. ASME*, Ser. H, Vol. 88, 1966, pp. 1–12.
12. Mager, A., *Generalization of Boundary Layer Momentum Integral Equation to Three-Dimensional Flows Including Those of Rotating System.* NACA TR 1067, 1952.
13. Spannhake, W., *Proc. Nat. Conf. Ind. Hydraulics*, Vol. 8, October 1944.
14. Ludwieg, H., *Ing. Arch.*, Vol. 19, No. 296, 1951.
15. Mullan, P. J., *An Investigation of Cavitating Inducers for Turbopumps.* M.I.T., Gas Turbine Lab Report 53, May 1959.
16. Bosch, H. B., et al., *Advanced Inducer Study.* ER-5288, NASA Document N63–21124, TRW, Inc., May 1963.
17. Sandercock, D. M., et al., *Cavitation and Noncavitation Performance of an 80.6° Flat Plate Inducer.* NACA TN D1439, November 1962.

18. SOLTIS, R. F., ET AL., *Investigation of the Performance of a 78° Flat Plate Helical Inducer.* NACA TN D1170, March 1962.
19. VAVRA, M. H., *Aerothermodynamics and Fluid Flow in Turbomachines.* John Wiley and Sons, Inc. (New York), 1960, p. 123.
20. MCCAFFERTY, H. G., *Errors in Measuring the Fluctuating Flow at the Discharge of an Inducer.* M.S. thesis, Dept. Aerospace Eng., Penn State U., June 1967.
21. LAKSHMINARAYANA, B., *Investigations and Analysis of Flow in Axial Flow Inducer.* NASA CR 103291, June 1969.
22. SMITH, L. H., *Three-Dimensional Flow in Axial Flow Turbomachinery.* Johns Hopkins U., Report I–14, November 1953.
23. SCHWARZ, W. H., AND C. A. FRIEHE, *Deviations from Cosine Law for Yawed Cylindrical Anemometer Sensors.* ASME Paper 68–WA/APM–16.
24. LAKSHMINARAYANA, B., Visualization Study of Flow in Axial Flow Inducer. *J. Basic Eng.*, Dec. 1972, p. 777–787.

DISCUSSION

G. F. WISLICENUS (Tucson, Arizona): I am very happy to discuss this paper, as I was connected for a considerable length of time with the work on which this paper reports.

Our friends from NASA will recall that we had no illusions about the inherent difficulties of this investigation at the time it was proposed. As I recall it, we stated in this proposal that real-flow effects were expected to extend over the *entire* flow field. In other words, we expected to find a mess, and this expectation was certainly fulfilled. The objective we had in mind was not only to learn something about rocket pump inducers, but equally to learn how to deal with such a complex and theoretically almost hopeless flow problem. It may be understandable why an old engineer like myself might want to get involved in such a problem. But it commands my respect when a younger engineer and scientist like Dr. Lakshminarayana is willing to struggle for years with this type of investigation, and even more so if he finally comes up with results that seem to make sense. I can assure you that while I was still at Penn State I found hardly any time to contribute to this often frustrating work. And now I am completely out of it, which has given Dr. Lakshminarayana the opportunity to pursue his investigation in a more undisturbed fashion.

I do not feel qualified to discuss the author's theoretical investigations except for the observation that some of the comparisons between his theoretical and experimental results impress me as much closer than I personally would have expected. But if it is really true, as stated in conclusion (2), that frictional effects in inducers are now predictable, then it is our obligation to put this knowledge in a form that can be used by the practical designer. After all, if friction effects double or triple the head generated in the tip regions, then their consideration is a plain necessity in the design process.

There is only one point I should like to discuss in a little more detail; i.e., that according to figures 11 and 18 the angular momentum of the flow *seems* to decrease with increasing distance from the impeller. The statement that this is due to "mass flow redistribution" might not be a sufficient explanation for some old-fashioned engineers like myself. It seems to me that this situation could be cleared up by plotting the circumferential velocity component (V_θ) against the stream function of the (circumferentially averaged) meridional flow, as the local angular momentum transport is, after all, proportional to the local mass flow. If

such a plot still shows a decrease in angular momentum, this decrease must be explained by a circumferentially nonuniform mass and momentum exchange between the positive flow region and the backflow region.

In passing, I should like to ask whether the axial velocity curves shown in figure 16 satisfy the condition of continuity. To check this, it might be interesting to plot the same curves against r^2, considering the backflow areas as negative. It illustrates the measuring problem before us if we mention that under such complex conditions of flow measurement any check on the validity on the results obtained is most welcome.

It worries me just a little that the simple throttle valve which I suggested to use might have an upstream effect that could influence the separation at the hub downstream of the inducer. This possibility could be checked with relative ease.

J. E. CROUSE (NASA Lewis Research Center): The author and investigators associated with this project should be congratulated on the depth of their research work. It is encouraging to see some "in depth" studies among the large number of papers published these days.

In the paper, considerable effort was made to construct models of velocity profiles and loss mechanisms. The data essentially confirms that suspected significant radial profiles near the blade surfaces do indeed exist. One of the more interesting results of the work is the small effect these radial components have on the predicted energy addition as evidenced by the $\overline{V_\theta}/U_t$ profiles of figure 15 with and without the radial velocity terms.

The important empirical term in the author's flow prediction equation is the term representing the loss gradient. Especially for low flow coefficient turbomachines, such as inducers, a good flow prediction method is highly dependent on an accurate representation of the loss gradient. The source of the losses is not important for the prediction method itself, but knowledge of the source of the losses can be rather important in setting up a reasonable loss model. The author chose to correlate all the losses associated with the flow through an inducer into a pipe-type friction parameter for the relative flow channel.

The experimental data of figure 9 for several rotors, according to the author's suggested correlation, is indeed somewhat better than that of figure 8, which is the same data by another correlation. The better correlation of loss data should be considered one of the most important results of this work.

J. H. HORLOCK (Cambridge University): To one who has attempted to predict the averaged flow in conventional axial flow turbomachines, this is a fascinating paper in that the method of attack has to be entirely different for several reasons.

(1) The axial velocity term in the radial equation of motion $W_z(dW_z/dr)$ is neglected because of the high stagger of the blade.

(2) Prediction of the tangential velocity distribution $W_\theta(r)$ instead of $W_z(r)$ is attempted.

(3) Variations of velocities across the pitch due to viscous effects are important.

(4) The radial loss distribution is dominant (although this is also important in axial-flow compressors at low flow coefficients).

I have followed B. Lakshminarayana's work with interest and discussed it with him. But there are still several aspects of the investigation that are not clear to me.

(1) On what basis is it justifiable to neglect $\partial W_z/\partial r$ compared with $\partial W_r/\partial z$?

(2) In the region near the blade in the outer half of the rotor, I think the magnitude of the radial body force due to viscous loss should be estimated. It is of order of magnitude $[\tan\alpha\,\partial(\Delta P_0/\rho)/\partial x]$ and may not be negligible.

(3) Why is the loss correlation improved by including the flow coefficient ϕ? I would expect it to be related to $(\phi-\phi_{\text{design}})$ but not simply as inverse of ϕ.

(4) The change in $\overline{V_\theta}(r)$ with r (fig. 11) is mysterious. Is it possible to measure the torque on the rotor and compare it with the change of tangential velocity across the rotor, in order to see if there are errors in the measurement of the latter.

Undoubtedly this work will be of use to designers of other turbomachines, especially in the prediction of performance at low ϕ. Has the author any recommendations on how the design of the inducer may be modified to allow for the observations of this paper? Can the large increase in loss with radius be avoided, and is the operation of the outer part as a drag pump inevitable? Or should the inner part be designed inviscidly and the outer part as a drag pump?

P. COOPER (Case Western University and TRW Inc.): Dr. Lakshminarayana's work makes one aware of the strong three-dimensional effects that serve to alter the expected performance of an inducer. He has made us aware of heretofore unexplained radial flows and other effects of the highly frictional flow that exists in an inducer. That he has been able to predict the outlet tangential velocity distribution by using his new loss scheme is especially encouraging.

I would like to inquire about the flow process connected with his predicted shift in this tangential velocity distribution from that of design. The author suggests that the flow action near the inducer tip is like that of a shear force pump. Is there a way that he could illustrate this more

fully? One possible explanation for this phemonenon at the tip is that the much higher loss there would result in too low a pressure—were it not for the action of the blades in maintaining radial equilibrium. Accordingly, the outlet tangential velocity component becomes quite large at the tip in an effort by the machine to produce more work there to offset this loss. Now, regardless of the blade-to-blade and hub-to-shroud velocity profiles, is not this process the result of guidance by the blades? Is the tip axial velocity component still connected with the tangential component through the blade angle there?

F. F. ANTUNES (Ingersoll Rand Inc.): Since the testing was done as a free impeller (without a stator or guide vanes), there is some question as to whether the three-dimensional effects are greatly exaggerated from that of an inducer with stator downstream. It is suggested that a reasonable stator be added and velocities remeasured.

LAKSHMINARAYANA (author): I would like to thank the discussors for their helpful comments and criticisms.

Professors Wislicenus and Horlock have commented on the mysterious effect; i.e., large change in angular momentum as the flow proceeds downstream. The author explained that this is due to large redistribution of mass flow that occurs downstream of the inducers. This can be explained from the following calculations. To check the accuracy of the measurements, area averaged axial velocity $\overline{V_z}$ and mass averaged $\overline{V_\theta}$ are computed at the measuring stations using the following equations.

$$\frac{\overline{V_z}}{U_t} = \frac{2}{1-R_h^2} \int_{R_h}^{1} \frac{V_z}{U_t} R \, dR$$

$$\frac{\overline{V_\theta}}{U_t} = \frac{\int_{R_h}^{1} \frac{V_\theta}{U_t} \frac{V_z}{U_t} R \, dR}{\int_{R_h}^{1} \frac{V_z}{U_t} R \, dR}$$

The values of $\overline{V_z}/U_t$, $\overline{V_\theta}/U_t$ at various measuring stations (see fig. 10) are shown in table D–I.

As can be seen from table D–I, the accuracy of V_z measurements, which is within 4 percent, is better than expected in such a flow. The change in mass averaged $\overline{V_\theta}$ is small compared to local changes observed at various stations (compare fig. 11 and table D–I). This confirms the author's conclusions that local V_θ changes are brought about mainly by flow redistribution. The mass averaged V_θ shows a consistent trend in that it decreases continuously downstream, the decrease being small

TABLE D–I.—*Values of* $\overline{V_z}/U_t$, $\overline{V_\theta}/U_t$ *at Various Stations*

Station number	4	5	6	7
$\frac{\overline{V_z}}{U_t}$	0.076	0.0775	0.0745	0.0775
$\frac{\overline{V_\theta}}{U_t}$	0.346	0.326	0.306	0.26

everywhere except between stations 6 and 7. The reasons for this are mentioned by Wislicenus. Some of the discrepancy in $\overline{V_\theta}$ may also be due to experimental inaccuracy in measuring the flow in the backflow region, whose extent extends up to 20 percent of annulus at station 7.

To check whether a simple throttle valve used in these experiments has any effect on inducer flow, especially in inducing backflow at the hub region, measurements were carried out with a properly designed throttle as shown in the insert in figure D–1. The tests were carried out with a *three-bladed inducer*, since this geometry was readily available. Please note that all the measurements reported in this paper are carried out in a *four-bladed inducer* and *hence velocity profiles plotted in figures D–1 and 16 are for different solidity inducers.* The results shown in fig. D–1 indicate that the throttle has no effect on flow separation at the blade trailing edge and its influence is felt only beyond station 6, which is far downstream of the inducer. Thus, it is concluded that the throttle has no effect on flow separation observed at stations 3, 4, and 5, even though the extent of backflow is somewhat reduced at station 6.

The author agrees with Mr. Crouse with regard to the source of the losses. Knowledge of the source of losses is extremely important in the design of inducers where incorporation of viscous effects is a necessity. The group at Penn State is now engaged in understanding the various sources of losses. This would lead to an analytical model which recognizes various mechanisms responsible for flow departure and losses.

In regard to Professor Horlock's comment on the magnitude of the body force term due to viscous losses, I have proved below that its magnitude is extremely small and its neglect in the equations of motion is justified.

Since the radial equilibrium equation used in this paper is passage averaged, it is necessary to find the average (blade to blade) of the body force term due to viscous losses. This term is thus equal to

$$\overline{F_{d_r}} = \int_0^1 \frac{\partial}{\partial x}\left(\frac{\overline{\Delta P_0}}{\rho}\right)\frac{W_r}{W_x}\,d\eta \tag{36}$$

$$\simeq \frac{1}{3} \tan \alpha \frac{\partial}{\partial x} \left(\frac{\overline{\Delta P_0}}{\rho} \right) \tag{37}$$

(from equation (13)).

In deriving equation (37), it is assumed that the streamwise gradient of local loss in P_0 is nearly the same as the corresponding gradient of average loss in P_0. Using equation (21), it can be proved that

$$\overline{F_{d_r}} \sim \frac{1}{3} \lambda_R \overline{W} \frac{\partial \overline{W}}{\partial x} \tan \alpha \tag{38}$$

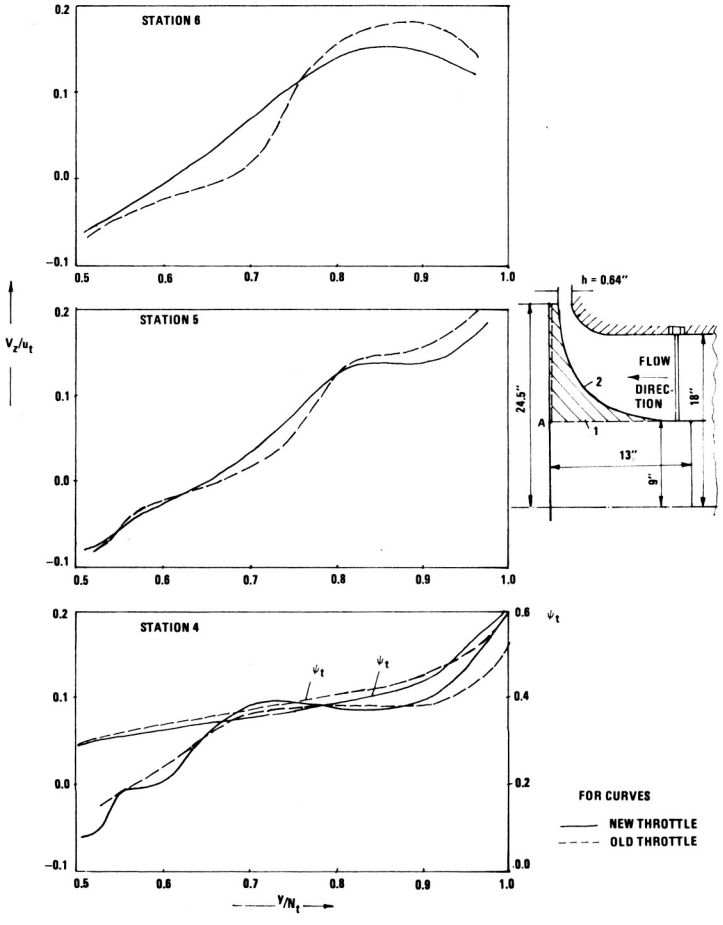

FIGURE D–1.—*Radial variation of* V_z/U_t *and* ψ_t *at various axial stations with simple (old) and aerodynamically designed (new) throttle (three-bladed inducer).*

since

$$\frac{L}{d_h} \sim \frac{1}{\cos \beta}$$

and

$$\frac{\partial}{\partial r}\left(\frac{\overline{\Delta P_0}}{\rho}\right) \sim \frac{\lambda_R}{r_t}\,\overline{W}\,\frac{\partial \overline{W}}{\partial R} + \frac{\overline{W}^2}{2r_t}\,\frac{\partial \lambda_R}{\partial R} \tag{39}$$

Hence the ratio of the two terms is

$$\frac{\overline{F_{d_r}}}{\dfrac{\partial}{\partial r}\left(\dfrac{\overline{\Delta P_0}}{\rho}\right)} = \frac{r_t \lambda_R \dfrac{\partial \overline{W}}{\partial x} \tan \alpha}{3\left(\lambda_R \dfrac{\partial \overline{W}}{\partial R} + \dfrac{\overline{W}}{2}\dfrac{\partial \lambda_R}{\partial R}\right)} \tag{40}$$

This ratio is evidently very small as illustrated in this example (using measured values).

At $R = 0.8$, $\tan \alpha = 0.36$ (from fig. 13)

$\lambda_R = 0.19$, $\dfrac{\partial \lambda_R}{\partial R} = 2.1$ (from fig. 9)

$\overline{W} = 0.6 U_t$, $\dfrac{\partial \overline{W}}{\partial R} = 0.6 U_t$ (from fig. 14)

$\dfrac{\partial \overline{W}}{\partial x} = \dfrac{-0.05 U_t}{r_t}$ (fig. 9 and eq. (27))

Substituting these values in equation (40), we get

$$\frac{\overline{F_{d_r}}}{\dfrac{\partial}{\partial r}\left(\dfrac{\overline{\Delta P_0}}{\rho}\right)} \simeq 1.5 \times 10^{-3}$$

Hence the body force term neglected in my analysis is extremely small compared to $\partial/\partial r(\overline{\Delta P_0/\rho})$ and its neglect is certainly justified. Even at the tip, where $\partial \overline{W}/\partial R$ is negative, the ratio is extremely small since $\partial \lambda_R/\partial R$ is very large and α is very small.

The other comment by Professor Horlock concerns the choice of the parameter ϕ in the loss correlation. The physical reasoning behind this choice is that at lower ϕ (which means larger stagger angles) narrower blade passages result and thus the flow in these passages becomes fully

developed sooner and hence viscous effects become larger. I don't agree with Professor Horlock that $\phi - \phi_{design}$ should be the parameter. Unlike a compressor aerodynamicist, an inducer hydrodynamicist is faced with the dilemma of evaluating the losses even at the design conditions where the frictional losses are several orders of magnitude higher than those in a compressor. It is the intention of the author to understand the design flow first and then attempt to correlate the flow losses at off-design conditions.

The physical flow process occurring within the inducer is more complex than explained by Dr. Cooper. Larger increase in V_θ and absolute head rise is not due to guidance of the blade. The flow deviation angles are found to be large at every radial location. As explained in this paper, the radial velocities are large and are of the same order of magnitude as the axial components. Under these circumstances, the inducer should be treated as a mixed flow pump. The meridional component (in the viscid flow) through the inducer can be divided into axial and radial components. The axial component can be treated in the manner described by Dr. Cooper, but the radial component of the flow makes the inducer behave as a shear force pump. The author is presently investigating the possibility of predicting the flow by this approach.

With regard to the comment by Mr. Antunes, it is very doubtful that a stator or guide vane would improve the flow through the inducer. On the other hand, large flow redistribution that occurs downstream of the inducer may be controlled, to some extent, by means of a stator. From physical and mathematical considerations, it is very hard to see how a stator would change the three-dimensional viscous character of the flow inside the inducer.